Journal of Power Sources 202 (2012) 284–290

Contents lists available at SciVerse ScienceDirect

Journal of Power Sources

journal homepage: www.elsevier.com/locate/jpowsour

Well-ordered spherical $LiNi_xCo_{(1-2x)}Mn_xO_2$ cathode materials synthesized from cobolt concentration-gradient precursors

Zhenlei Huang, Jian Gao*, Xiangming He, Jianjun Li, Changyin Jiang

Institute of Nuclear and New Energy Technology, Tsinghua University, Beijing 100084, PR China

ARTICLE INFO

Article history:
Received 6 August 2011
Accepted 26 October 2011
Available online 25 November 2011

Keywords:
Lithium-ion batteries
Cathode materials
NMC materials
Concentration-gradient
Ordered

ABSTRACT

Spherical $Ni_xCo_{(1-2x)}Mn_x(OH)_2$ (x = 0.333, 0.4, 0.416, 0.45) precursors with Co concentration-gradient were prepared by co-precipitation from sulfate solutions using NaOH and NH_4OH as precipitation and complexing agents. Then, well-ordered spherical $LiNi_xCo_{(1-2x)}Mn_xO_2$ was synthesized by sintering the mixture of as-prepared precursor and Li_2CO_3 at 950 °C for 16 h in air. EDXS results indicated that the concentration of cobalt decreased gradually inside out of the spherical precursor particle, and it was uniform in spherical $LiNi_xCo_{(1-2x)}Mn_xO_2$ particle obtained by sintering with Li_2CO_3. According to Rietveld refinement of XRD patterns, the $LiNi_xCo_{(1-2x)}Mn_xO_2$ synthesized from Co gradient precursor showed lower degree of cation disorder than that prepared from conventional precursor. The well-ordered $LiNi_xCo_{(1-2x)}Mn_xO_2$ from Co gradient precursor delivered much better high-rate capability than conventional one. The decrease of cation disorder of $LiNi_xCo_{(1-2x)}Mn_xO_2$ is attributed to the cobalt-rich in core of the precursor particles. Both abundant Co^{3+} and Li^+ can restrain cation mixing effectively. Since Li^+ needs long time to reach core during calcining, cobalt-rich in core of the precursor particle is very important for restraining cation mixing. Concentration-gradient precursor is helpful to prepare well-ordered $LiNi_xCo_{(1-2x)}Mn_xO_2$ with good high-rate capability, and the total content of expensive and toxic cobalt does not need to be increased.

1. Introduction

Ternary materials $LiNi_xCo_{(1-2x)}Mn_xO_2$ with a layered $NaFeO_2$ structure has been studied extensively as cathode materials for rechargeable lithium-ion batteries because of their high reversible capacity, wide working voltage range, low cost and good thermal stability [1–4]. The transition metal ions (TM) in this kind of materials are Ni^{2+}, Co^{3+}, and Mn^{4+} [5–8]. Mn^{4+} can raise the structural and thermal stability, but it is almost electrochemical inactive in the charging/discharging process. The most charge/discharge capacity of material is contributed by the oxidation and deoxidation of Ni^{2+}/Ni^{4+}, especially under 4.4 V [9]. But it is harmful to the thermal stability and cycle performance that Ni is excessive in $LiNi_xCo_{(1-2x)}Mn_xO_2$ [10]. Besides, Ni^{2+} (r = 0.69 Å) and Li^+ (r = 0.76 Å) have similar ionic radius, and they tend to exchange their sites in crystal cell, which is referred to as cation disorder or cation mixing. Because of that, the nominated structure of $(Li)_{3a}[Ni_xCo_{(1-2x)}Mn_x]_{3b}\{O_2\}_{6c}$ is in fact $(Li_{1-y}Ni_y)_{3a}[Li_yNi_{(x-y)}Co_{(1-2x)}Mn_x]_{3b}\{O_2\}_{6c}$ [11–13]. In this structure, Ni^{2+} will block the diffusion path of Li^+ on Li^+ plane due to the electrostatic repulsion of Li^+ and Ni^{2+}, which is harming to the rate capability of $LiNi_xCo_{(1-2x)}Mn_xO_2$ [14].

Increasing the amount of lithium and cobalt in $LiNi_xCo_{(1-2x)}Mn_xO_2$ is an effective way to restrain cation mixing [15,16]. Excess lithium will lead to the oxidation of part of Ni^{2+} to smaller Ni^{3+} (r = 0.56 Å), and the lacking of lithium inclines to break of lithium layer. In preparing process, 3–11% excess lithium is usually introduced. In contrary to excess of Li^+, increasing cobalt contention in $LiNi_xCo_{(1-2x)}Mn_xO_2$ is more outstanding way to restrain cation disorder. When x = 0.5, 12% Li^+ exchange their sites with Ni^{2+}, and less than 2% Ni^{2+} are found in lithium layer when x = 0.25 [16–18]. However, more cobalt will results in economical and environmental problems because cobalt is rather costly and toxic. Minimizing cation mixing without increasing Co usage will be commercially valuable.

Gradient material has been studied as cathode material for lithium ion batteries. Sun et al. prepared $Li(Ni_{0.8}Co_xMn_{0.2-x})O_2$ material with core–shell structure. The concentration of Mn in shell of particle was higher than that in core, which was just inverse for concentration of Ni [19,20]. The electrochemical properties and thermal stability of the core–shell $Li(Ni_{0.8}Co_xMn_{0.2-x})O_2$ material were improved, which was attributed to the Mn^{4+} and Ni^{2+} concentration-gradient distribution. Koenig et al. also synthesized the tailored $Li_{1.2}(Mn_{0.62}Ni_{0.38})_{0.8}O_2$ particles with internal gradient

* Corresponding author. Tel.: +86 10 89796078; fax: +86 10 89796031.
E-mail address: gaoj@mail.tsinghua.edu.cn (J. Gao).

0378-7753/$ – see front matter © 2011 Elsevier B.V. All rights reserved.
doi:10.1016/j.jpowsour.2011.10.143

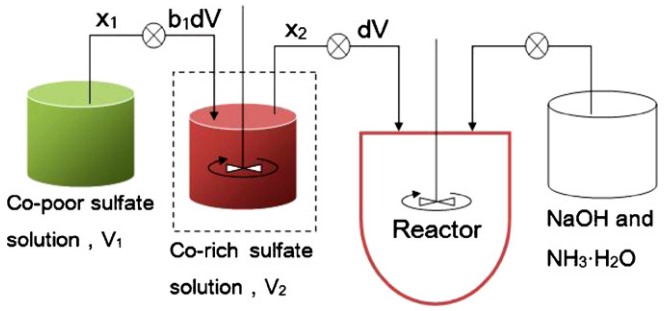

Fig. 1. Illustration of co-precipitation process.

of Ni and Mn. Mn was rich on surface of particle and Ni was rich in core [21].

$LiNi_xCo_{(1-2x)}Mn_xO_2$ is commonly synthesized by solid-state reaction of $Ni_xCo_{(1-2x)}Mn_x(OH)_2$ precursor and LiOH or Li_2CO_3 at high temperature. LiOH or Li_2CO_3 particles are firstly adhered on the surface of precursor particles, and then Li^+ diffuses into the core of precursor particle during calcining. In this work, spherical $Ni_xCo_{(1-2x)}Mn_x(OH)_2$ (x = 0.333, 0.4, 0.416, 0.45) precursors with Co concentration-gradient were firstly synthesized by improved co-precipitation. Co was rich in core and the Co concentration was decreased inside out of the precursor particle. Well-ordered spherical $LiNi_xCo_{(1-2x)}Mn_xO_2$ was then prepared from this precursor. Effects of gradient precursor on the cation disorder and electrochemical performance of $LiNi_xCo_{(1-2x)}Mn_xO_2$ were studied in detail.

2. Experimental

Taking $Ni_{0.4}Co_{0.2}Mn_{0.4}(OH)_2$ as example, spherical gradient precursor was synthesized as follows. The solution of $NiSO_4$ (Sinopharm Chemical Reagent, China) and $MnSO_4$ (Sinopharm Chemical Reagent, China) (Ni:Mn = 1:1, molar ratio) was named solution A. The solution of $NiSO_4$, $CoSO_4$ (Sinopharm Chemical Reagent, China), and $MnSO_4$ (Ni:Co:Mn = 3:4:3, molar ratio) was named solution B. Solution A was pumped into solution B in flow rate Q. Simultaneously, the mixed solution of A and B was agitated vigorously and pumped continuously into a water-jacketed CSTR reactor in flow rate 2Q. The reactor was filled with N_2. The volume of solutions A and B was equal and two solutions were exhausted at the same time. In this way, concentration of cobalt fed into the reactor was decreased continuously. The solution of NaOH (Sinopharm Chemical Reagent, China) and $NH_3{\cdot}H_2O$ (Sinopharm Chemical Reagent, China) was also pumped into the reactor at the same time. $NH_3{\cdot}H_2O$ acted as chelating agent. The pH value and temperature were controlled at about 11.0 and 50 °C in the reactor, respectively. The stirring speed was about 1500 rpm min^{-1}. After 2 h, all operations were stopped for 20 min and the precipitation deposited entirely in the reactor. Part of supernatant liquid, which volume was equal to the volume of solution B pumped into the reactor in 2 h, was drawn out and the volume was emptied for next 2 h reaction. All the raw solutions were completely pumped into the reactor in about 20 h. Then the final product in the reactor was filtered, washed and dried in turn. Thus, the spherical gradient $Ni_{0.4}Co_{0.2}Mn_{0.4}(OH)_2$ powders were obtained. The co-precipitation process was illustrated in Fig. 1. The conventional precursors with no concentration-gradient of TM were also prepared by the same method.

The spherical $LiNi_{0.4}Co_{0.2}Mn_{0.4}O_2$ was synthesized by sintering the mixture of as-prepared precursor and Li_2CO_3 (Sinopharm Chemical Reagent, China) at 950 °C for 16 h in air. 7 at.% excess of Li_2CO_3 was added to compensate the loss in calcining process.

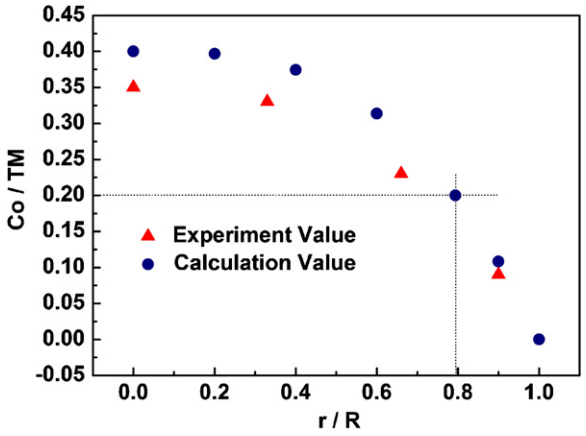

Fig. 2. Co concentration gradient in $Ni_{0.4}Co_{0.2}Mn_{0.4}(OH)_2$ particle by calculating and testing.

The molar ratio of metal elements in material was evaluated by inductively coupled plasma (ICP) emission spectroscopy. The XRD patterns were recorded by Rigaku D/MAX-2500 X-Ray Diffractometer with Cu-K radiation (λ = 1.54056 Å) in the range of 10–100° with a step size of 0.03°. Rietveld refinements were carried out with the FullProf suite program (Windows version, April 2004) to acquire crystal parameters and degree of cation mixing. The particle morphology of the powders were observed using a scanning electron microscopy equipped with an EDAX energy disperse X-ray spectrometer (SEM, JSM6301F).

2032-type coin cells for electrochemical tests were assembled in a glove box filled with dry argon gas. The cathode consisted 80 wt.% $LiNi_xCo_{(1-2x)}Mn_xO_2$ material, 10 wt.% acetylene black as conducting agent, and 10 wt.% polyvinylidene fluoride (PVdF) as binder. After being uniformly blended in *N*-methylpyrrolidinone, the electrode was pressed in the form of a disk with a diameter of 9 mm and then dried at 120 °C for 24 h in vacuum. A typical cathode disk contained active material of about 12 mg cm^{-2}. Celgard 2400 microporous membrane was used as separator and lithium metal served as anode. The electrolyte was 1 mol L^{-1} $LiPF_6$ EC + DEC (1:1 volume ratio). Charge and discharge tests were galvanostatically performed at different C-rates with 1.5 mA as 1C in the potential range of 2.7–4.5 V (versus Li/Li^+) at room temperature.

3. Results and discussion

3.1. Preparation and characterization of $Ni_xCo_{(1-2x)}Mn_x(OH)_2$ precursors

Spherical $Ni_xCo_{(1-2x)}Mn_x(OH)_2$ precursors with Co concentration-gradient were prepared by co-precipitation. The concentration gradient distribution of cobalt in precursor particle was achieved by inteqrally feeding-in. The sketch of inteqrally feeding-in and reaction was shown as Fig. 1. The concentration of cobalt fed to reactor was calculated by the molar balance of Co of input–output, as follows.

As shown in Fig. 1, V_1 is initial volume of Co-poor solution, x_1 is Co molar concentration of a species in the Co-poor solution, V_2 is initial volume of the Co-rich solution, x_2 is initial Co molar concentration of Co-rich solution fed to the reactor, V is the volume of the sulfate solution fed to the reactor in the time of t, x is molar concentration of Co fed to the reactor at the time of t, and dV is the volume of the solution fed to the reactor in the time of dt.

$$b_1 = \frac{V_1}{V_1 + V_2} = \frac{V_1}{V_0} \quad (1)$$

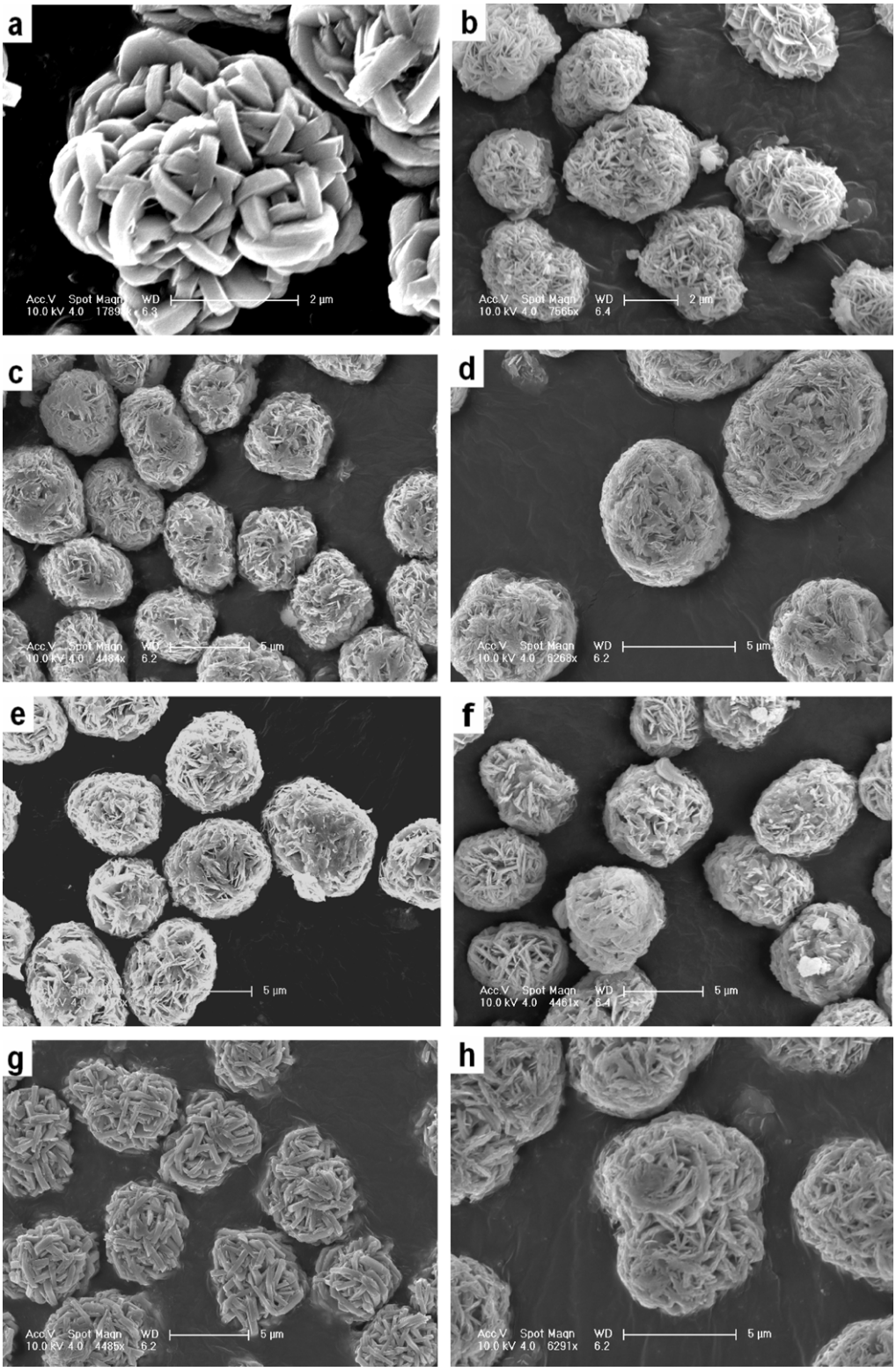

Fig. 3. SEM images of $Ni_xCo_{(1-2x)}Mn_x(OH)_2$ powders. U10, (b) G10, (c) U17, (d) G17, (e) U20, (f) G20, (g) U33, and (h) G33.

$$b_2 = \frac{V_2}{V_1 + V_2} = \frac{V_2}{V_0} \tag{2}$$

A molar balance on the Co-rich solution (labeled by dashed line in Fig. 1) as a function of V results in the following expression.

$$x_1 b_1 \, dV - x\, dV = (b_2 V_0 - V + b_1 V)dx + x \, dV \tag{3}$$

When the V changes from 0 to V, x decreases from x_2 to x. Applying the boundary condition to Eq. (3) results in following expression:

$$x = \left(1 - \frac{V}{V_0}\right)^{b1/b2} (x_2 - x_1) + x_1 \tag{4}$$

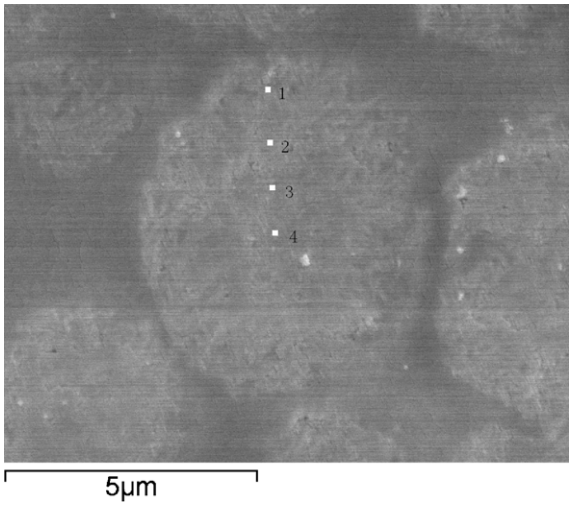

Fig. 4. SEM image of the cross-section of $Ni_{0.4}Co_{0.2}Mn_{0.4}(OH)_2$ particle.

If $V_1 = V_2$, $b_1 = b_2$ and $x_1 = 0$, then

$$x = \left(1 - \frac{V}{V_0}\right) x_2 \quad (5)$$

Eq. (5) indicates that Co concentration in Co-rich sulfate solution decreases linearly over time. The concentration of Co deposited on the particles decreases along with the decreasing of the Co concentration of solution fed into the reactor. Thus, the Co-concentration gradient is formed in the precursor particles. The Co concentration distribution in $Ni_{0.40}Co_{0.20}Mn_{0.40}(OH)_2$ precursor particle was calculated and tested, as shown in Fig. 2. R is final radius of the particle and r is real-time radius in the process of precipitation. As can be seen from Fig. 2, the concentration of Co decreases slowly between $r/R = 0$–0.5. The position $r/R = 0.794$ is the half point of the volume of the particle, which means that a thin shell layer occupies the half volume and 50% Co exists in this rather thin shell if Co distributes uniformly in particle. When $r/R < 0.794$, the concentration of Co is higher than average concentration (Co-rich area). When $r/R > 0.794$, the concentration of Co is lower than average concentration (Co-poor area). It is worth noticing that the feeding way adopted in this paper can obviously result sharp gradient of Co concentration across the radius of precursor particle.

Gradient $Ni_xCo_{(1-2x)}Mn_x(OH)_2$ ($x = 0.33$, 0.4, 0.416, 0.45) are signed as G33, G20, G17, G10, and corresponding conventional precursors are signed as U33, U20, U17 and U10, respectively. In co-precipitation process, primarily fine particles were firstly formed, which was the cores of the final precursor particles. Then, the fresh hydroxide precipitated on these cores and the particles grew up gradually. Finally, spherical precursor particles were yielded. The SEM images of precursors are shown in Fig. 3. The particle size of $Ni_{0.45}Co_{0.1}Mn_{0.45}(OH)_2$ precursor powder is about 3–4 μm. Other precursors have a larger diameter of 5–6 μm.

The EDXS test shows that the molar ratio of Co/TM on the surface of G20 precursor particle is 0.065:1, which is higher than calculation value because the area detected by probe beam of EDXS is under the particle surface. The cross-section of G20 particle was also tested by EDXS. As shown in Fig. 4, the points collected EDXS spectra are labeled as 1, 2, 3 and 4 from outside in, which is probably corresponding to the positions of $r/R = 0.9$, 0.6, 0.3, and 0, respectively. The Co-concentration distribution tested by EDXS is shown in Fig. 2. Agreed with the theoretically prediction, Co is mainly concentrated in the centre of the particle and little Co is appeared near the particle surface. However, the tested Co concentration is lower than calculation value in centre of the particle, and it is just high near the surface. The deviation between experimental and calculated values may come from following reasons. The precursor particles are porous secondary particles, which are not uniformly piled with the primary fine particles. Some fresh precipitation with low concentration of Co can come into the core through the cracks of particle. Besides, the Co concentration tested by EDXS represents an average value in the bulk around the selected point and EDXS testing has itself unavoidable errors [21]. The actual compositions of all precursors acquired from ICP-AES are listed in Table 1. The ICP results coincide well with theoretical prediction.

3.2. Characterization of $LiNi_xCo_{(1-2x)}Mn_xO_2$

The $LiNi_xCo_{(1-2x)}Mn_xO_2$ cathode materials were synthesized by calcining the mixture of $Ni_xCo_{(1-2x)}Mn_x(OH)_2$ precursor and Li_2CO_3 at 950 °C for 16 h in air. Corresponding to the precursors of G33, G20, G17 and G10, the products are named LG33, LG20, LG17 and LG10, respectively. Similarly, LU33, LU20, LU17 and LU10 materials come from U33, U20, U17 and U10 precursors, respectively. The SEM images of $LiNi_xCo_{(1-2x)}Mn_xO_2$ powders are shown in Fig. 5. LG and LU samples are all spherical and have narrow particle size distribution. The Co/TM ratios on the particle surface were also analyzed by EDXS. As shown in Table 1, in contrast to the precursor particles, the Co/TM ratio on the surface of LG10, LG17, LG20, LG33 particles rises to 10.2%, 16.8%, 19.8%, and 32%, which indicates the Co concentration-gradient disappears in final lithiated materials.

Fig. 6 shows the XRD diffraction profiles of $LiNi_xCo_{(1-2x)}Mn_xO_2$ from different precursors. All the peaks are indexed as typical hexagonal phase with space group R-3m. Rietveld refinement of $LiNi_xCo_{(1-2x)}Mn_xO_2$ is performed by using $(Li_{1-z}Ni_z)_{3a}[Ni_{x-z}Co_{1-2x}Mn_x]_{3b}\{O_2\}_{6c}$ structural model. The main structural parameters obtained from the refinement are summarized in Table 2. The agreement factors of refinements show that the calculated patterns agree well with the observed patterns. The cell parameters of a and c are both reduced when the Co content is increased in $LiNi_xCo_{(1-2x)}Mn_xO_2$. This is because that the radius of Co^{3+} (0.545 Å) is less than that of Ni^{2+} (0.69 Å), and similar with Mn^{4+} (0.53 Å) [16]. So, along with the increasing of Co content, average radius of TM decreases, which results in the shrink of crystal cell. The parameters of a and c also decrease with the decreasing of cation mixing. As shown in Fig. 7, LG samples have less cation mixing than LU samples.

The well cation order may be resulted from the Co concentration-gradient in the precursor particle. When the precursor and Li_2CO_3 are calcined, the precursor particles are surrounded by plenty of Li^+ and Li^+ diffuses very slowly to the core of the particles. So the concentration of Li^+ is high on shell and low in the core of particles during calcining process. When $Ni_xCo_{(1-2x)}Mn_x(OH)_2$ with cobalt concentration gradient is used as precursor, the concentration of Co is sufficient in the core, although where Li^+ is little. Since high Co concentration is effective for reducing cation mixing as abundant Li^+, enough strong force are supplied to restrain cation mixing both in shell and core of particle. The effect of cobalt concentration-gradient on cation disorder is more remarkable for large particle since Li^+ more slowly diffuses to the centre of particle. Although the Co concentration gradient disappears after calcination, the benefit of well cation order resulted by gradient precursor is retained, which is confirmed by the XRD refinement. The solid-state reaction process using gradient precursor is illustrated in Fig. 8

.

The intensity ratio of $I(003)/I(104)$ can reflect the degree of cation disorder for layered structure $LiNi_xCo_{(1-2x)}Mn_xO_2$. A high value of $I(003)/I(104)$ means low degree of cation disorder and good electrochemical performance. Conversely, if value of $I(003)/I(104)$ is lower than 1.1, the cation disorder is undesirable, which indicates that a few Ni^{2+} are mixed with Li^+ in 3a sites [22,23].

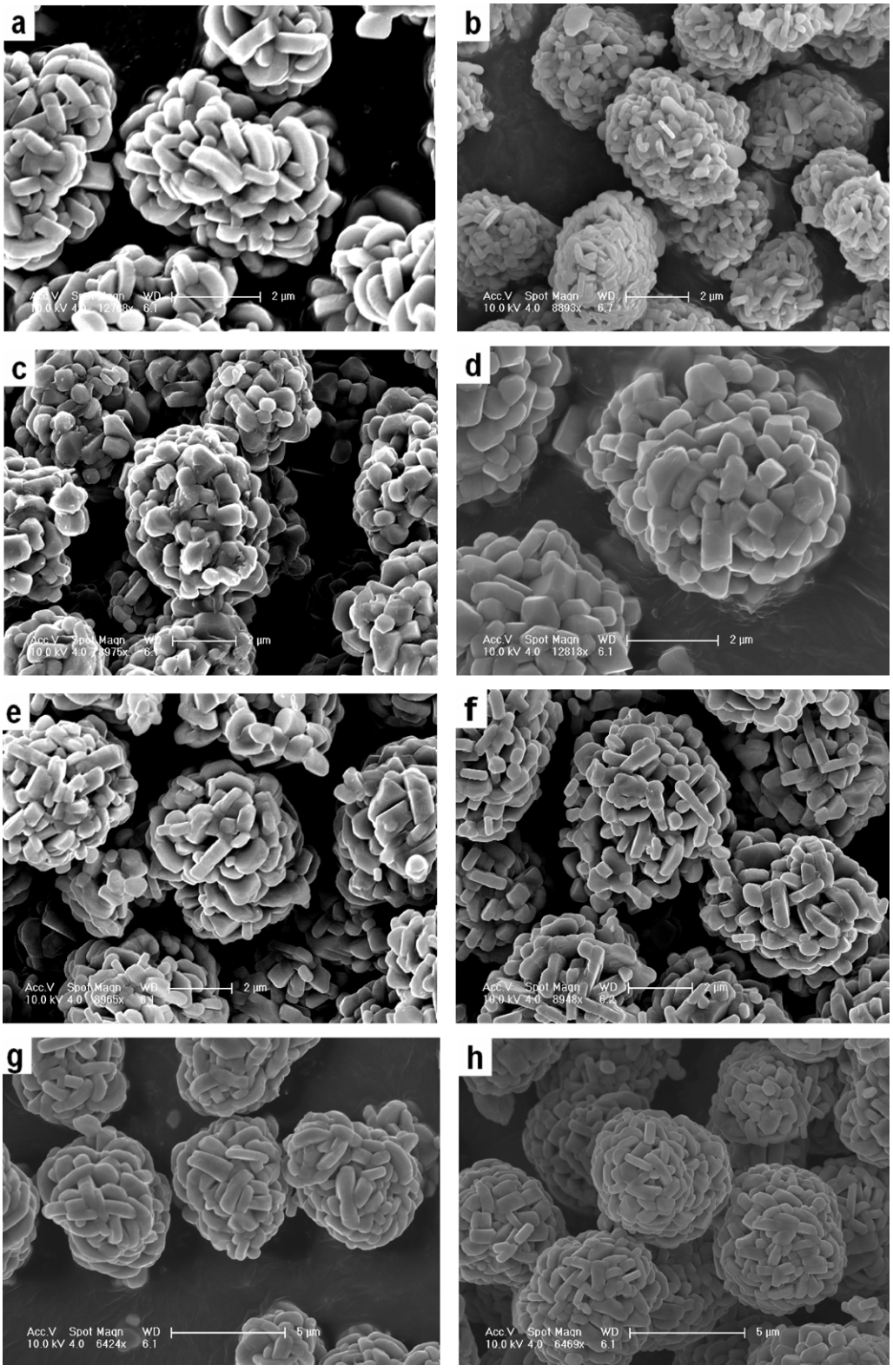

Fig. 5. SEM images of $LiNi_xCo_{(1-2x)}Mn_x(OH)_2$. LU10, (b) LG10, (c) LU17, (d) LG17, (e) LU20, (f) LG20, (g) LU33, and (h) LG33.

The variation of $I(003)/I(104)$ ratio with Co/TM ratio is shown in Fig. 9. The $I(003)/I(104)$ of LG samples are obviously greater than that of LU samples. The R value, defined as the ratio of the intensity of doublet peaks (006) and (102) to (101) peak, is meanwhile an indicator of the extent of hexagonal ordering. Material with good hexagonal ordering usually has an R value of lower than 0.5. The R value is lower, the hexagonal ordering is better [14,24,25]. R values of samples are less than 0.5 except LU10 and R decreases with the increasing of molar ratio of Co/TM. Compared with LU samples, LG samples show lower R values when the Co concentration is same, which means that LG samples have more perfect hexagonal structure. R and $I(003)/I(104)$ ratio are listed in Table 2.

Table 1
Actual composition of gradient $Ni_xCo_{(1-2x)}Mn_x(OH)_2$ and Co/TM on the surface of precursors and $LiNi_xCo_{(1-2x)}Mn_xO_2$ particles.

Sample name	Nominal composition	Actual composition	Co/TM on the surface of precursor (%)	Average Co/TM of $LiNi_xCo_{(1-2x)}Mn_xO_2$ (%)
U10	$Ni_{0.45}Co_{0.10}Mn_{0.45}(OH)_2$	$Ni_{0.440}Co_{0.091}Mn_{0.469}(OH)_2$	–	–
G10		$Ni_{0.450}Co_{0.091}Mn_{0.459}(OH)_2$	3.9	10.2
U17	$Ni_{0.416}Co_{0.168}Mn_{0.416}(OH)_2$	$Ni_{0.410}Co_{0.173}Mn_{0.417}(OH)_2$	–	–
G17		$Ni_{0.412}Co_{0.176}Mn_{0.412}(OH)_2$	9.7	16.8
U20	$Ni_{0.40}Co_{0.20}Mn_{0.40}(OH)_2$	$Ni_{0.393}Co_{0.202}Mn_{0.405}(OH)_2$	–	–
G20		$Ni_{0.392}Co_{0.198}Mn_{0.410}(OH)_2$	6.5	19.6
U33	$Ni_{0.33}Co_{0.34}Mn_{0.33}(OH)_2$	$Ni_{0.325}Co_{0.342}Mn_{0.333}(OH)_2$	–	–
G33		$Ni_{0.325}Co_{0.341}Mn_{0.334}(OH)_2$	9.9	32.0

Table 2
The structure parameters of $LiNi_xCo_{(1-2x)}Mn_xO_2$ samples.

Sample name	a (Å)	c (Å)	c/a	$I(003)/I(104)$	R	Cation disorder (%)	R_p (%)	R_{wp} (%)	χ^2	R_b (%)
LU10	2.8766	14.2682	4.957	0.99	0.516	7.2	11.8	14.2	3.28	2.148
LG10	2.8753	14.2615	4.958	1.00	0.470	6.7	12.7	14.4	3.47	2.886
LU17	2.8749	14.2645	4.962	1.02	0.489	6.3	10.7	12.5	2.56	1.903
LG17	2.8710	14.2545	4.965	1.09	0.477	5.3	9.09	11.5	2.19	1.787
LU20	2.8693	14.2536	4.968	1.13	0.432	4.1	12.9	13.8	2.62	1.852
LG20	2.8685	14.2498	4.968	1.17	0.411	3.6	12.8	14.7	3.13	2.092
LU33	2.8619	14.2343	4.976	1.12	0.416	4.0	11.3	14.3	2.92	2.316
LG33	2.8605	14.2284	4.974	1.27	0.400	3.1	10.7	14.1	2.89	2.604

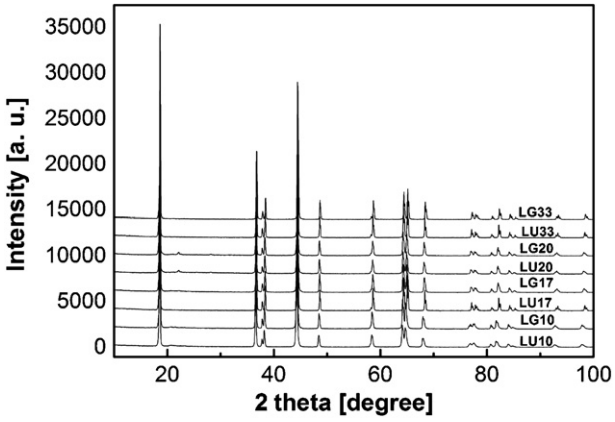

Fig. 6. XRD patterns of $LiNi_xCo_{(1-2x)}Mn_xO_2$ from different precursors.

In summarize, values of $I(003)/I(104)$, R, and degree of cation disorder all demonstrate that LG samples have more regular hexagonal structure and less cation disorder than LU samples. Therefore, LG samples are expected better electrochemical performance.

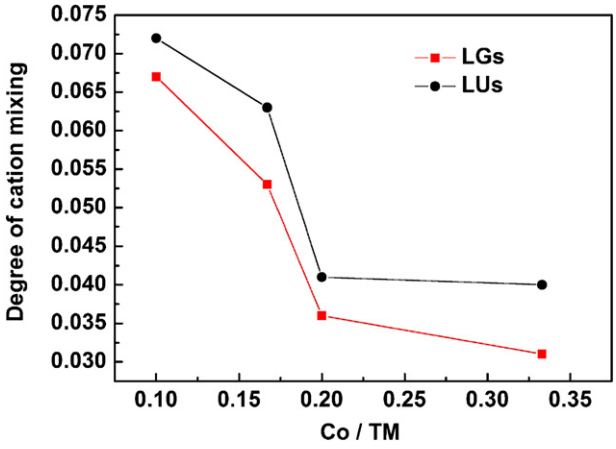

Fig. 7. Cation mixing of $LiNi_xCo_{(1-2x)}Mn_xO_2$ from different precursors.

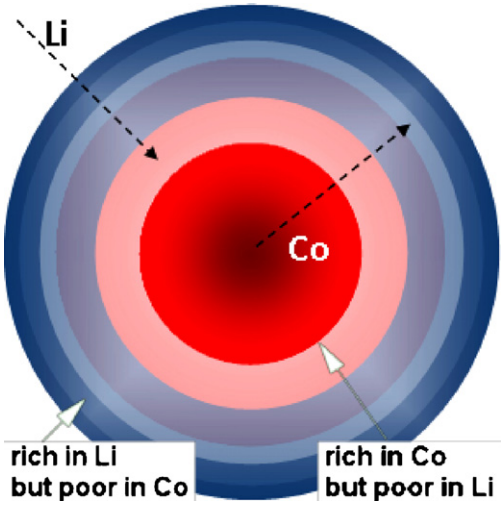

Fig. 8. Illustration of solid-state reaction process.

3.3. Electrochemical performance of $LiNi_xCo_{1-2x}Mn_xO_2$

Electrochemical properties of $LiNi_xCo_{1-2x}Mn_xO_2$ cathode materials were investigated using coin type cell. The cells were charged and discharged twice at 0.2C rate, then charged at 1C and discharged at 1C, 2C, 3C and 5C rates for 5 cycles, respectively. The test results are shown in Fig. 10. The typical discharge capacities at different rates are given in Table 3. As shown in Fig. 10 and Table 3, the rate capabilities of LG samples are remarkably higher than that of LU samples at over 1C rate, which is owed to the low degree of cation mixing and regular layered hexagonal

Table 3
Typical discharge capacities of LG and LU samples at 1C, 2C, 3C, and 5C rates.

C-rates	Typical capacity of the samples (mAh g^{-1})							
	LU10	LG10	LU17	LG17	LU20	LG20	LU33	LG33
1C	141.9	148.1	147.4	163.7	163.7	170.5	162.4	176.8
2C	124.2	133.7	135.6	151.4	145.4	156.8	150.1	167.3
3C	110.3	122.0	126.3	144.9	134.4	147.3	144.7	162.6
5C	90.5	107.5	116.1	129.8	115.2	128.8	135.1	153.6

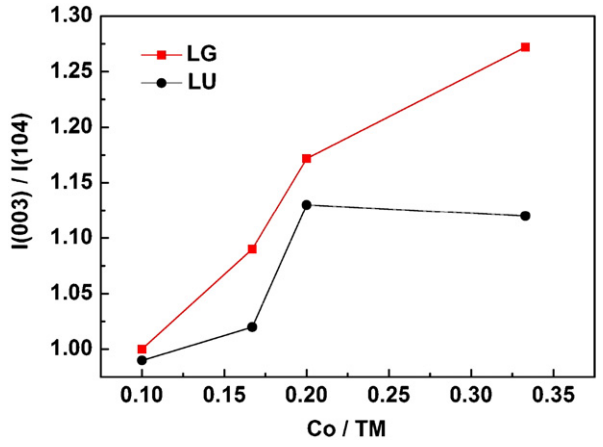

Fig. 9. $I(003)/I(104)$ of $LiNi_xCo_{(1-2x)}Mn_xO_2$ from different precursors.

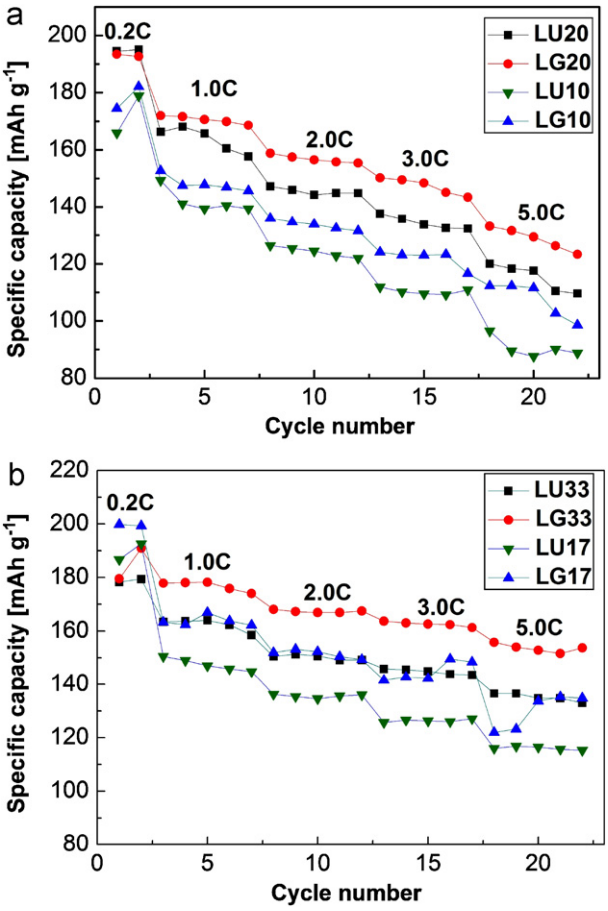

Fig. 10. Rate capability of (a) $LiNi_{0.45}Co_{0.1}Mn_{0.45}O_2$, $LiNi_{0.40}Co_{0.20}Mn_{0.40}O_2$ and (b) $LiNi_{0.416}Co_{0.168}Mn_{0.416}O_2$, $LiNi_{0.333}Co_{0.333}Mn_{0.333}O_2$.

structure of LG samples. Because of less Ni^{2+} barriers and more ordered passway, Li^+ can unhinderedly diffuse in the crystal of LG samples. Thus the LG samples can exhibit excellent electrochemical performance at heavy currents. Although content of Co is halved, the rate capability of LG17 is comparable to LU33 at 1C, 2C, 3C and 5C. In contrast, the rate capability of LG10 is inferior to that of LU20. Although LG10 is prepared from gradient precursor, the degree of cation mixing is still as high as 6.7% because of the low Co content, which is higher than 4.1% of degree of cation mixing of LU20. The results reveal that gradient precursor is beneficial to synthesize $LiNi_xCo_{1-2x}Mn_xO_2$ materials with good electrochemical performance and the expensive and toxic cobalt can be decreased at the same time. The materials prepared from gradient precursors have great commercial competitiveness in the lithium-ion batteries market.

4. Conclusions

The spherical gradient $Ni_xCo_{(1-2x)}Mn_x(OH)_2$ precursors with Co-rich in core and Co-poor on surface have been prepared by proposed process. The well ordered spherical $LiNi_xCo_{(1-2x)}Mn_xO_2$ is synthesized from this cobalt concentration-gradient precursor, which shows a hexagonally ordered layered structure and low degree of cation mixing. Co-gradient in precursor can effectively restrain cation mixing in calcining process while the expensive and toxic cobalt is not increased. The $LiNi_xCo_{(1-2x)}Mn_xO_2$ material from gradient precursor exhibits better rate capability. Discharge capacities of $LiNi_{0.40}Co_{0.20}Mn_{0.40}O_2$ and $LiNi_{0.416}Co_{0.168}Mn_{0.416}O_2$ synthesized from gradient precursors are comparable to $LiNi_{0.333}Co_{0.333}Mn_{0.333}O_2$ obtained from conventional precursor at 1C, 2C, 3C, and 5C rates, although their Co contents are sharply decreased. The better electrochemical performance of $LiNi_xCo_{1-2x}Mn_xO_2$ prepared from gradient precursor is attributed to the low cation mixing and well ordered hexagonal structure. Spherical Co-gradient $Ni_xCo_{(1-2x)}Mn_x(OH)_2$ material prepared in this work is a promising precursor for synthesizing $LiNi_xCo_{(1-2x)}Mn_xO_2$ cathode materials.

Acknowledgements

This work is supported by a grant from National Basic Research Program of China (973 Program) (Project No. 2011CB935902). We also thank Feng Qi of Department of Material Science and Engineering, Tsinghua University, for the great help in the preparation of EDXS samples.

References

[1] Y. Bentaleb, I. Saadoune, K. Maher, et al., J. Power Sources 195 (2010) 1510.
[2] H.J. Lee, K.S. Park, Y.J. Park, J. Power Sources 195 (2010) 6122.
[3] C. Deng, S. Zhang, B.L. Fub, et al., J. Alloys Compd. 496 (2010) 521.
[4] X. Zhang, A. Maugera, Q. Lu, et al., Electrochim. Acta 55 (2010) 6440.
[5] Z. Lu, D.D. MacNeil, J.R. Dahn, Electrochem. Solid-State Lett. 4 (2001) A200.
[6] D.D. MacNeil, Z. Lu, J.R. Dahn, J. Electrochem. Soc. 149 (2002) A1332.
[7] J.M. Kim, H.T. Chung, Electrochim. Acta 49 (2004) 937.
[8] N. Tran, L. Croguennec, M. Menetrier, et al., Chem. Mater. 20 (2008) 4815.
[9] D. Liu, Z. Wang, L. Chen, Electrochim. Acta 51 (2006) 4199.
[10] J. Ying, C. Wan, C. Jiang, J. Power Sources 102 (2001) 162.
[11] K.M. Shaju, G.V. Subba Rao, B.V.R. Chowdari, Electrochim. Acta 48 (2002) 145.
[12] Y. Koyama, I. Tanaka, H. Adachi, et al., J. Power Sources 119–121 (2003) 644.
[13] J. Xiao, N.A. Chernova, M.S. Whittingham, Chem. Mater. 20 (2008) 7454.
[14] K.K. Cheralathan, N.Y. Kang, H.S. Park, et al., J. Power Sources 195 (2010) 1486.
[15] S. Venkatraman, J. Choi, A. Manthiram, Electrochem. Commun. 6 (2004) 832.
[16] K. Shizuka, T. Kobayashi, K. Okahara, et al., J. Power Sources 146 (2005) 589.
[17] S.W. Oh, S.H. Park, C. Park, et al., Solid State Ionics 171 (2004) 167.
[18] D. Li, H. Noguchi, M. Yoshio, Electrochim. Acta 50 (2004) 427.
[19] Y. Sun, S. Myung, B. Park, et al., Nat. Mater. 8 (2009) 320.
[20] Y. Sun, D. Kim, H. Jung, et al., Electrochim. Acta 55 (2010) 8621.
[21] G.M. Koenig Jr., I. Belharouak, et al., Chem. Mater. 23 (2011) 1954.
[22] J. Kim, P. Fulmer, A. Manthiram, Mater. Res. Bull. 34 (1999) 571.
[23] T. Ohzuku, A. Ueda, M. Nagayama, et al., Electrochim. Acta 38 (1993) 1159.
[24] J.N. Reimers, E. Rossen, C.D. Jones, et al., Solid State Ionics 61 (1993) 335.
[25] G.T.K. Fey, J.G. Chen, Z.F. Wang, et al., Mater. Chem. Phys. 87 (2004) 246.